Werk

Jahr: 1985
Kollektion: fid.geo
Signatur: 8 Z NAT 2148:56
Digitalisiert: Niedersächsische Staats- und Universitätsbibliothek Göttingen
Werk Id: PPN1015067948_0056
PURL: http://resolver.sub.uni-goettingen.de/purl?PPN1015067948_0056

LOG Id: LOG_0024
LOG Titel: Static deformations and gravity changes at the earth's surface due to atmospheric loading
LOG Typ: article

Übergeordnetes Werk

Werk Id: PPN1015067948
PURL: http://resolver.sub.uni-goettingen.de/purl?PPN1015067948
OPAC: http://opac.sub.uni-goettingen.de/DB=1/PPN?PPN=1015067948

Contact

Niedersächsische Staats- und Universitätsbibliothek Göttingen
Georg-August-Universität Göttingen
Platz der Göttinger Sieben 1
37073 Göttingen
Germany
Email: gdz@sub.uni-goettingen.de

J Geophys (1985) 56:81–99

Journal of Geophysics

Static deformations and gravity changes at the earth's surface due to atmospheric loading

W. Rabbel and J. Zschau
Institut für Geophysik, Christian Albrechts Universität, Olshausenstr. 40–60, D-2300 Kiel, Federal Republic of Germany

Abstract. Deformations and gravity changes at the Earth's surface due to regional and global air pressure variations are estimated for a radially stratified earth. The results are as follows:
– *Vertical displacements* of seasonal character have maximum amplitudes of ± 0.5 cm. (Anti-)Cyclones, however, can cause vertical displacements of up to ± 2.5 cm.
– *Horizontal displacements* have amplitudes less than ± 2.5 mm.
– *Horizontal principal strains* may have amplitudes up to 10^{-8}. They reduce to about $\pm 1.5 * 10^{-9}$ for seasonal changes in the air pressure distribution.
– The *total gravity perturbation* consisting of the Newtonian attraction of air masses and of self-gravitation due to the elastic deformation may go up to ± 20 μgal in the case of (anti-)cyclones, and ± 3 μgal in the case of seasonal air pressure changes.
– The *total tilt* due to seasonal air pressure variations can be as high as ± 1.5 mseca. For passing (anti-)cyclones this value may go up to ± 10 mseca.

All the above values have to be modified in the direct vicinity of coastlines. The modification is only slight for the displacements and the secondary gravity effect, but it is important for the other components. There, the necessary modification may amount to several hundred percent depending on the type of deformation component and on the distance to the coastline.

Precise air pressure corrections of radial displacements and gravity changes cannot be achieved by using a single regression coefficient. Either the characteristic wavelengths of the pressure distribution have to be taken into account or the following two-coefficient correction equations have to be used:

Radial displacement: $u = -0.90\,\tilde{p} - 0.35\,(p - \tilde{p})$
Primary gravity: $g_p = 0.36\,\tilde{p} + 0.41\,(p - \tilde{p})$
Secondary gravity: $g_s = -0{,}17\,\tilde{p} - 0.08\,(p - \tilde{p})$
Total gravity: $g = g_p + g_s$,

with u = radial displacement in mm, g_p, g_s, g = primary, secondary and total gravity, respectively, in μgal, p = local pressure variation in mbar, $\bar{p}$ = average of the pressure variation in a surrounding area of 2,000 km (in mbar) and $\tilde{p}$ the same average, except for setting the pressure values equal to zero over ocean areas.

These corrections have been tested for seasonal air pressure variations and they have proved to be highly precise. The average errors are less than 0.5 mm, 0.1 μgal, 0.1 μgal and 0.2 μgal for the radial displacements, the primary, secondary and total gravity changes, respectively. The maximum errors are less than 1 mm in the case of the radial displacements, 0.3 μgal and 0.2 μgal for the primary and secondary gravity changes, respectively, and 0.4 μgal for the total gravity changes. Due to a small, spatially constant error term these values apply strictly only to spatial differences of the above deformation components. The differences, however, can be taken between any two points on the Earth's surface.

Key words: Geodynamics – Atmospherical loading – Global deformation – Global positioning – Gravity variations

Offprint requests to: W. Rabbel

Introduction

Global deformations of the Earth involving significant gravity changes may be caused by either endogenic, tectonic forces or by exogenic influences such as Earth tides, ocean and atmospheric loading as well as snow coverage during winter. The classical approach of measuring these phenomena is the use of continuously recording gravimeters, tilt- and strainmeters distributed over the Earth's surface. However, this approach has one principle difficulty: because of instabilities of the instruments and their installations it can only provide reliable information on periodic deformations of periods not much longer than one day. Thus, its applicability is almost exclusively restricted to the Earth's tidal deformation. This situation has improved significantly with the development of the superconducting gravimeter (Prothero and Goodkind, 1972) and it has drastically changed with the application of geodetic space techniques such as Satellite Laser Ranging and Very Long Baseline Interferometry (Committee on Geodesy, National Research Council, 1981).

Using the latter technique for relative positioning, even the direct determination of continental drift rates of the order of centimetres per year appears to become possible in the very near future. Preliminary results have already given continental drift rates over the last 3 years which generally agree with those averaged over the geological past (Walter, 1984). Millimeter-scale accuracies are envisaged for similar systems to detect vertical surface motions associated with tectonic processes (Walter 1984). High-precision relative gravimetry, as well as absolute gravimetry, promises to substantially contribute to achieving this goal. These

methods as well as the space techniques do not suffer from the above-mentioned lack of stability. Thus, besides measuring displacements due to continental drift, they will also correctly record long-period displacements as, for instance, those caused by seasonal changes in the Earth's surface load. Not allowing for such externally induced deformations might, for instance, result in erroneous continental drift rates from relative positioning provided the displacements of external origin are of the same order of magnitude as those due to global plate motion.

The purpose of this paper is to give an idea of the magnitude of deformations and gravity changes caused by regional and global variations in the air pressure distribution. Displacements, horizontal principal strains, tilt and gravity effects are estimated quantitatively.

The next section deals with deformations of the Earth's surface due to *regional* air pressure variations which are quasi-periodic with a repetition time of several days. The effect of *global seasonal* deviations from mean atmospheric pressure is investigated in the following section and, finally, a simple but highly precise correction of radial displacements and gravity changes for air pressure variations is presented.

Deformations and gravity changes due to (anti-)cyclones

The loading functions

Cyclones and anticyclones are extreme air pressure lows and highs, respectively, showing deviations from mean atmospheric pressure (1,013 mbar) of at least some 10 mbar. The highest pressure observed for anticyclones is 1,080 mbar, which occurred in Siberia. The lowest value for non-tropical cyclones is about 925 mbar, while in the tropics the pressure may even fall below 900 mbar, (Baur 1948, Faust 1968). Both cyclones and anticyclones have spatial extensions between some hundred (tropical cyclones) and some thousand kilometres (continental anticyclones). Their duration is generally of the order of a few days and sometimes they can remain stable for weeks. Thus, inertia effects in the corresponding loading deformations can usually be neglected. An exception to this is the passage of cold or warm fronts, for which the characteristic times involved may be much shorter than 1 day (see Müller and Zürn 1983). However, such phenomena are not considered here.

In most cases the pressure distributions of (anti-)cyclones are geometrically simple. The isobars are near to being circular and, in a first approximation, the anomalous pressure may be described by the simple formula

$$p(r)=p_{max}*\exp(-r^2/r_0^2) \qquad (1)$$

(Trubytsin and Makalkin 1976).

Here r is the distance from the centre of the (anti-)cyclone, p_{max} is the maximum pressure anomaly at the centre, and r_0 the distance at which the anomaly has dropped to p_{max}/e ($e=2.718\ldots$).

For estimating the deformations and gravity changes at the Earth's surface due to the occurrence of (anti-)cyclones we have set r_0 to three characteristic values:

– $r_0=160$ km and 400 km, modelling "tropical cyclones" (steep pressure gradient, small spatial extension)
– $r_0=1{,}000$ km, modelling a "continental anticyclone" (small pressure gradient, large spatial extension).

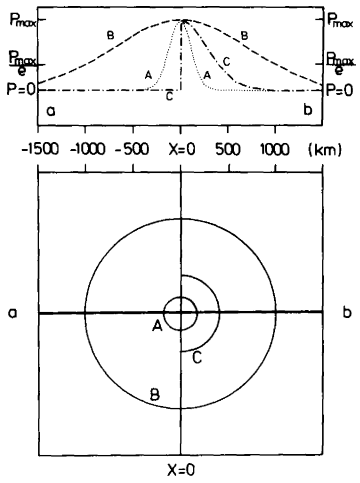

Fig. 1. Considered air pressure distributions. *Top:* Pressure amplitudes along profile a–b. *Bottom:* Two-dimensional distributions symbolized by *(half-)circles* with radius r_0, where r_0 denotes the distance at which the pressure anomaly has dropped to 1/e of the maximum value. (A) Continuous distribution as given by Eq. (1), with $r_0=160$ km (steep gradient, small extension of the pressure anomaly). (B) Continuous distribution as given by Eq. (1), with $r_0=1\,000$ km (small gradient, large extension of the pressure anomaly). (C) Discontinuous distribution as given by Eq. (2), with $r_0=400$ km and a coastline at $x=0$. Line a–b is the profile for which the deformation and gravity effects of Figs. 2–5 are calculated

All calculated deformations and gravity changes are normalized to $p_{max}=1$ mbar so that results for any maximum pressure can be readily deduced.

Strictly speaking, simple loading functions as given by Eq. (1) can only be applied to anomalous air pressure on the continental surface far from any coastlines. On the ocean floor, passing cyclones cause a more complicated effective pressure distribution due to the reaction of the water masses. In general, this reaction is dynamical and is affected by water depth, geometry of the coastlines, velocity of the cyclone etc., in a highly complex way. Without any dynamical effects the ocean would react to air pressure changes like an inverse barometer and would compensate an air pressure low by raising the water level such that there is no pressure change on the ocean floor. These static conditions are roughly valid for monthly mean values (Thompson 1979) or for very slow-moving cyclones.

To account for the static reaction of the ocean we have additionally used the anomalous pressure distribution

$$p_H=H(x-x_0)*p(r), \qquad (2)$$

where $p(r)$ is the same as in Eq. (1), $x=x_0=$const. defines a straight coastline and $H(x-x_0)$ is the Heaviside step function. Thus, there is zero pressure on the ocean side of the coastline and pressure distributions $p(r)$, as defined in Eq. (1), on the continental side.

Figure 1 shows the pressure distributions used in this section: two continuous distributions (Eq. 1) with $r_0=A,B$ and one discontinuous distribution (Eq. 2) with $r_0=C$ and $x_0=0$.

Method of calculation

The method of global loading calculations for a given Earth model and a given load distribution is now standard (see

Longman 1962; Farrell 1972; Zschau 1979a among others): loading love numbers are calculated first and from this the Earth's elastic response to a surface point load, the so-called Green's functions, are determined. The Green's functions are convolved with the load distribution in order to obtain the total displacements, strain, gravity and tilt effects for any desired point on the surface. The method takes account of self-gravitation and it usually involves a hydrostatic prestress term.

For the numerical evaluation of the convolution integrals we have used a grid system which is determined by meridians and parallels. All the Green's functions and loading distributions were taken as constant within one grid unit. The size of each grid unit was dependent on its distance to the surface point for which the loading calculations were carried out. However, it was always chosen such that a further refinement of the grid system did not change the results for any deformation component.

For the determination of the gravitational effects we have assumed the pressure variations to be due to a homogeneous perturbation of air density within a column of 8.4 km in height (standard atmosphere). The difference between the gravitational attraction of this upwards extending mass anomaly and the corresponding surface distribution of equal mass was taken into account by distance-dependent weighting functions.

Calculations have been carried out for a spherical and radially stratified Earth. We have used the Gutenberg-Bullen A Earth model as tabulated in Alterman et al. (1961). Test calculations with more up to date Earth models such as PREM (Dziewonski and Anderson 1981) did not give significantly different results. The introduction of anelasticity (see Zschau 1979c, d, 1980), however, may be important.

Estimates based on Q-model PREM and assuming $Q \sim \omega^{\alpha}$ (ω = circular frequency) with $\alpha = 0.15$ (see Smith and Dahlen 1981, Okubo 1982) gave an increase of the loading deformations by 10%–20% when seasonal air pressure variations were considered. But as the structure of anelasticity in the Earth's mantle and its frequency dependence is not sufficiently well known, we have not taken anelasticity into account.

Computational results

Figures 2–5 present the displacements, horizontal strain, gravity and tilt effects due to the surface pressure distributions A, B, C of Fig. 1. A, B, C are chosen to be 160 km, 1,000 km and 400 km, respectively. While the results in cases A and B are valid for any profile crossing the centre of the pressure anomaly, in case C they are valid along a profile perpendicular to the coastline (a–b perpendicular to $x = 0$ in Fig. 1).

As mentioned above, all values are normalised to 1 mbar pressure at the (anti-)cyclone's centre. In all cases, the direction pointing upwards is taken to be positive. Thus, contrary to the common notation, gravity will be positive if the attracting force is directed upwards. This ensures that only one coordinate system is used. Note the logarithmic scale of the length coordinate.

(a) Displacements (Fig. 2). In the case of continuous pressure distributions (A, B), the maximum displacements turn out to be in the range of $\mp$(1–2.5) cm for the vertical component and $\pm$(1–2.5) mm for the horizontal component. This assumes a maximum pressure anomaly between ± 20 and ± 60 mbar. The vertical component takes its extreme values at the centre of the (anti-)cyclone, the horizontal component at its flanks.

The magnitude of the displacements is critically dependent on the spatial extension r_0 of the pressure distribution. For instance, the vertical displacements for the $r_0 =$ 1,000 km pressure anomaly (B) are up to four times stronger than those of the $r_0 = 160$ km anomaly (A). From this it is clear that there cannot be any unique regression coefficient between local displacements and local air pressure changes which could be used to correct geodynamic measurements for air-pressure-induced surface displacements. The latter depend on the amplitude *as well as* on the spatial width of the pressure anomaly.

The introduction of a step function into the geometry of the load (C) modifies the displacements considerably; the symmetry with respect to the coastline ($x = 0$) is lost. Furthermore, the order of magnitude of the vertical displacements is the same as in case A although the width of pressure distribution A is less than half of the width of pressure distribution C. With the horizontal displacements, the order of magnitude is the same as in case B, although the width of pressure distribution B is more than twice as high as that of C. Thus, vertical displacements are weakened in the vicinity of a coastline, whereas horizontal displacements are amplified.

(b) Horizontal strains (Fig. 3). Figure 3 gives the horizontal principal strains along the profile a–b in Fig. 1. The maximum strain effects for the axial and azimuthal components corresponding to the continuous pressure distributions (A, B) are $\mp (4\text{–}12) * 10^{-9}$ if, as before, the pressure anomaly is assumed to be $\pm$(20–60) mbar at the centre of the (anti-)cyclone.

Compared to the displacements, the maximum amplitudes of the axial and azimuthal strains are not strongly determined by the width of the pressure distribution. The shape of the strain curves A, B is however, except for the sign, rather similar to that of the corresponding pressure curves. It suggests approximately $(-1.5) - (-2.0) * 10^{-10}$ strain per mbar of local air pressure change below the centre of the pressure anomaly. This coefficient, however, is not applicable to the flanks of the anomaly and it is not well enough determined to be used for precise air pressure corrections of geodynamic measurements.

The assumption of discontinuous surface pressure (C) leads to extremely high near-coast axial strain values (more than $-4 * 10^{-10}$ strain/mbar, with a change in sign at the location of the pressure discontinuity. The corresponding azimuthal strain component is described by a smooth curve similar to that for the vertical displacements.

(c) Gravity effect (Fig. 4). Each high and low pressure area corresponds to a density anomaly in the air. It causes an anomaly in the Newtonian attraction which is commonly known as the primary gravitational effect. The secondary gravitational effect of air pressure changes is due to the elastic deformation of the solid Earth. It includes gravity changes due to the shift of the surface through the gravity field and due to the redistribution of mass in the Earth's interior commonly known as self-gravitation.

A look at Fig. 4 demonstrates that the primary gravity

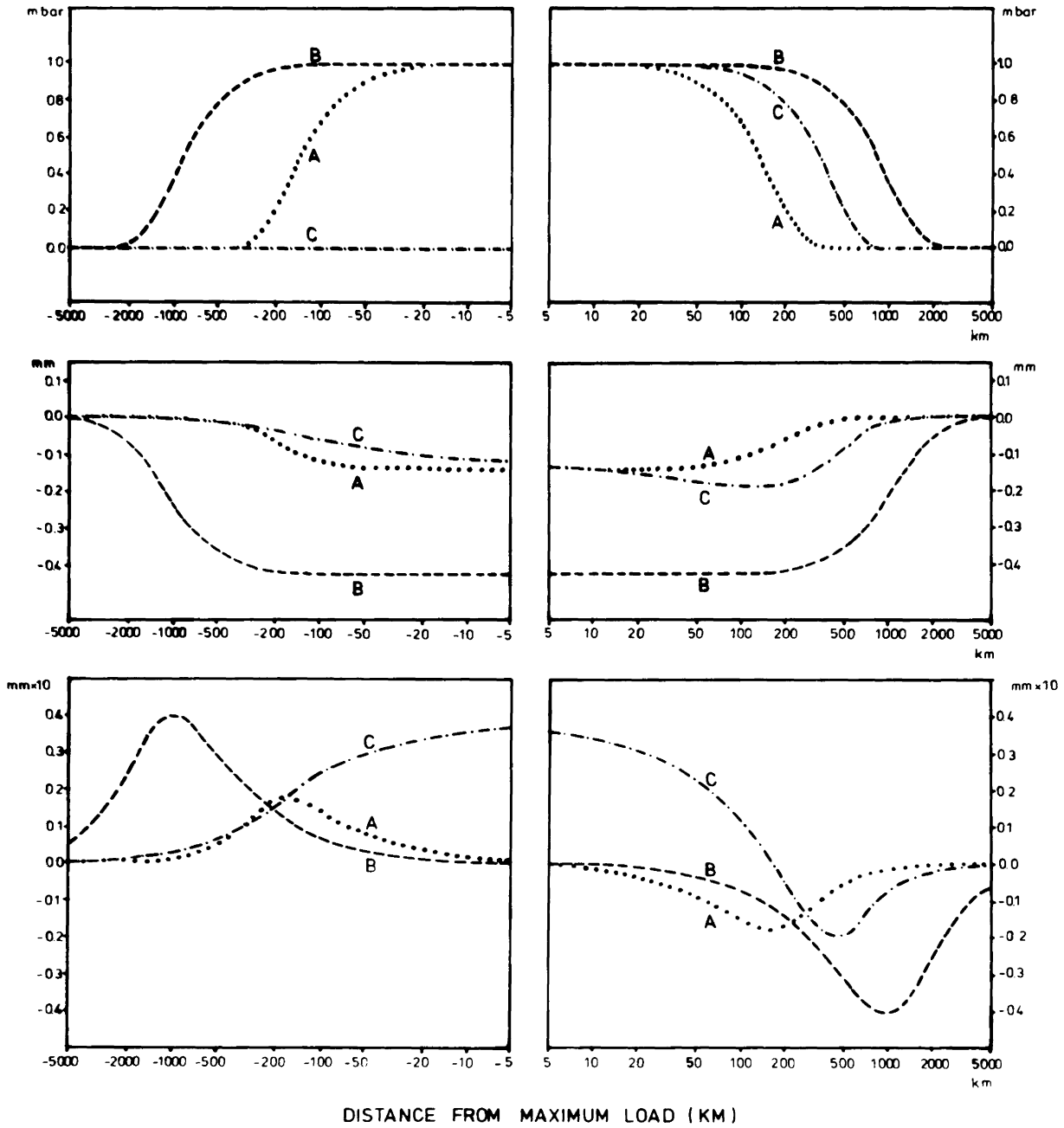

Fig. 2. *Top:* Axial cut through the anomalous air pressure distribution A, B, C of Fig. 1. *Middle:* Corresponding vertical displacement (positive upwards). *Bottom:* Corresponding horizontal displacements in the direction of profile a–b of Fig. 1

effect is dominant. It correlates remarkably well with the pressure variation. In the case of pressure distributions A and B, a good regression coefficient is 0.4 μgal/mbar. For the secondary gravitational effect such a correlation is not seen as clearly. Thus, in case of the total gravitational effect the regression coefficient for distributions A and B may vary between 0.3 and 0.4 μgal/mbar resulting in a gravity change of around ±20 μgal if, as before, a pressure change of ±60 mbar is assumed. The above regression coefficient is in good agreement with similar computations by Warburton and Goodkind (1977). It also agrees with the results obtained by Spratt (1982) who compared records of a superconducting gravimeter with local barometric pressure changes and came up with an averaged admittance of 0.29–0.34 μgal/mbar.

All results are based upon the assumption that the density perturbation is homogeneous within a standard atmosphere of 8.4 km in height and that the perturbation can be estimated from the surface pressure by means of the hydrostatic approximation.

A strong increase of the regression coefficient between air pressure variations and the primary gravity effect seems to occur under air pressure anomalies in ocean areas. Here, the coefficient goes up to 0.8 μgal/mbar (curve C). This amplification is due to the additional effect of water level changes caused by the static compensation of air pressure

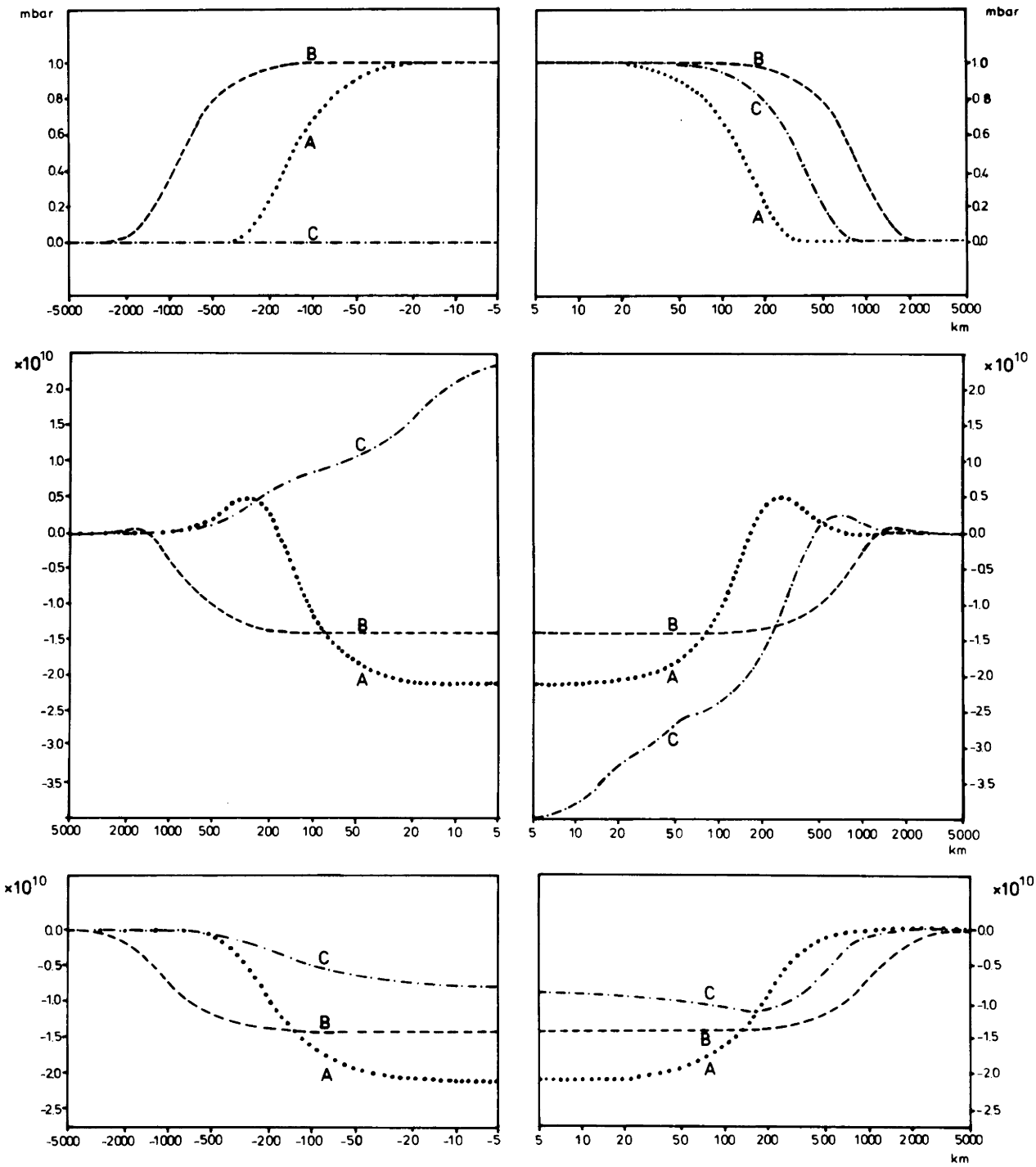

Fig. 3. *Top:* Axial cut through the anomalous air pressure distributions A, B, C of Fig. 1. *Middle:* Corresponding horizontal principal strain in the direction of profile a–b in Fig. 1 (axial strain). *Bottom:* Corresponding horizontal principal strain perpendicular to the direction of profile a–b in Fig. 1 (azimuthal strain). positive strain: increase of length (dilatation) negative strain: decrease of length (compression)

loading of the ocean. It will be measured by a gravimeter installed at mean sea level on a little island in the ocean whether the island is far from the coast or as near as 5 km to the next coastline. Only in the direct vicinity of the coastline is the regression coefficient lower and takes values between 0.8 and 0.4 μgal/mbar. This, however, neglects the height of the gravimeter station above mean sea level which, at coastal stations, may significantly change the above coefficient.

Comparing Fig. 4 with Fig. 2 one can also deduce a regression coefficient between air-pressure-induced vertical displacements and secondary gravity changes. On average it is 0.46 cm/μgal and is valid for both continuous (A, B) and discontinuous (C) pressure distributions. The corre-

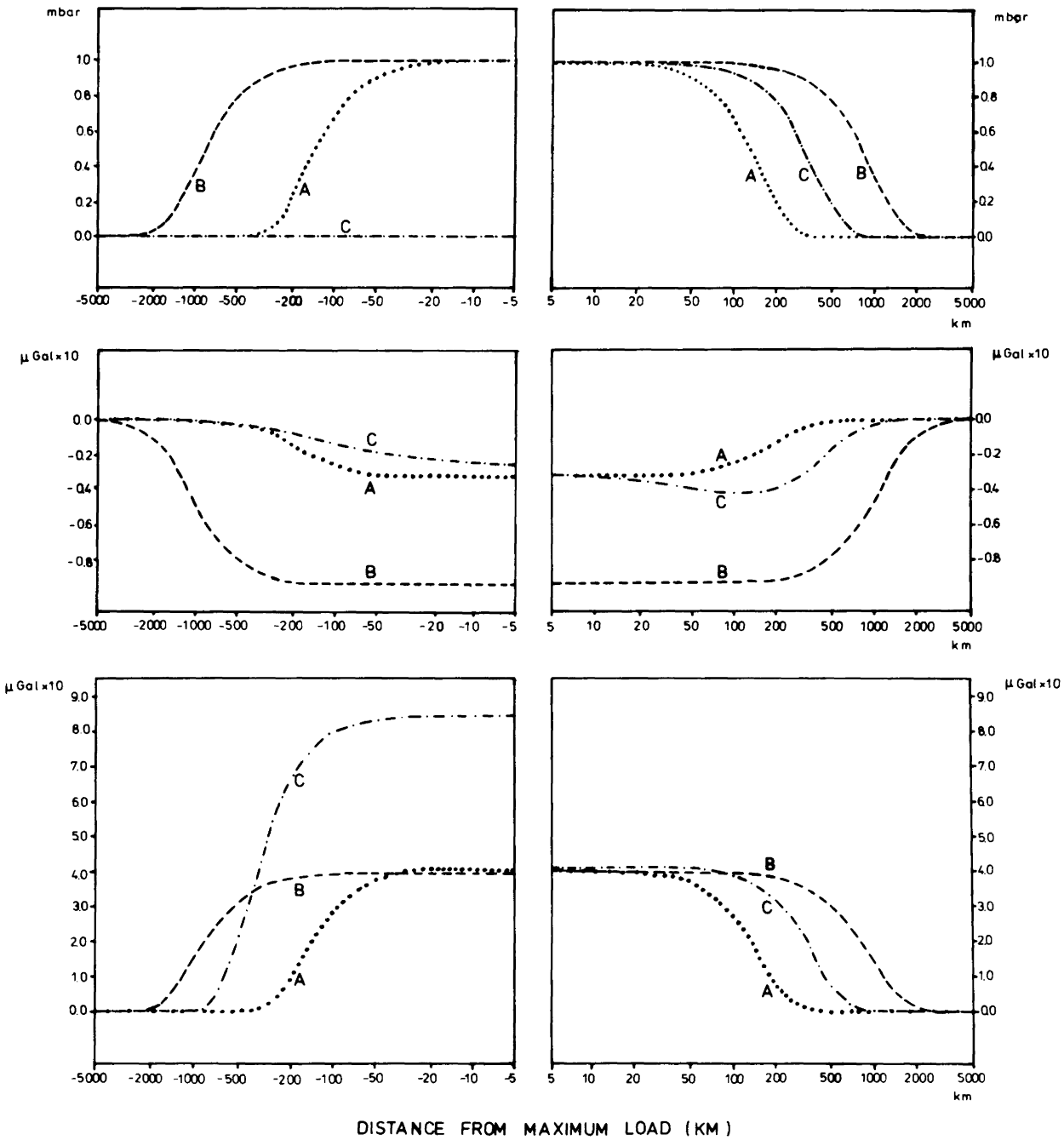

Fig. 4. *Top:* Axial cut through the anomalous air pressure distributions A, B, C of Fig. 1. *Middle:* Corresponding gravity effect caused by the elastic deformation (secondary effect). *Bottom:* Corresponding gravity effect caused by the Newtonian gravitation of the anomalous air mass (primary effect). Gravity is positive upwards!

sponding correlation is much better than that between the displacements and the air pressure variations. Unfortunately, such a good correlation is not obtained for the total gravity. Thus, the desired air pressure correction of global positionings with space techniques by means of gravity recordings would still require the difficult separation of the secondary gravity effect from the primary one.

(d) Tilt (Fig. 5). Similar to gravity, air-pressure-induced tilt consists of a primary effect, which is the deviation of the vertical due to the gravitational attraction of air, and a secondary effect which is the elastic deformation including the tilt of the surface and a secondary deviation of the vertical due to self-gravitation of the deforming Earth.

Contrary to gravity, the secondary tilt component is larger than the primary one. In the case of continuous pressure distributions (A, B) the extreme values of tilt are found under the flanks of (anti-)cyclones as in the case of horizontal displacements. In contrast to the displacements, however, the magnitude of the maximum tilt is less dependent upon the width of the pressure anomaly than upon the pressure gradient. Taking ± 20 mbar and ± 60 mbar again for the average and extreme pressure anomalies, respectively, in the centre of (anti-)cyclones, one obtains a maximum

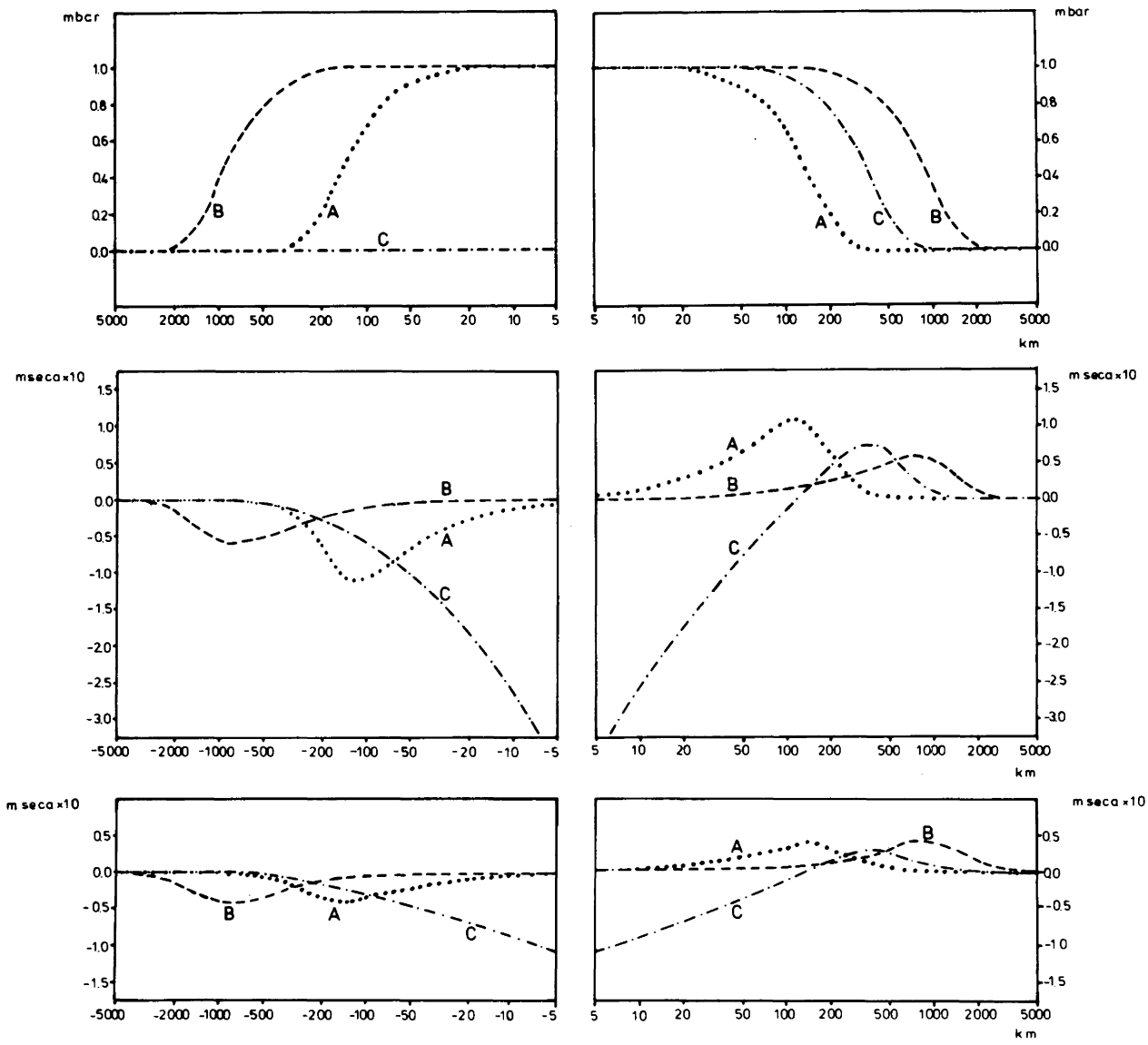

Fig. 5. *Top:* Axial cut through the anomalous air pressure distributions A, B, C of Fig. 1. *Middle:* Corresponding tilt caused by the elastic deformation (secondary effect). *Bottom:* Corresponding tilt (deflection of the vertical) caused by the Newtonian gravitation of the anomalous air mass (primary effect). All tilts are valid for the direction of profile a–b in Fig. 1 (positive, if the tip of a vertical pendulum moves into (-x)-direction)

tilt anomaly as high as $\pm$(3–10) mseca. For the discontinuous pressure distribution (C) this maximum increases by tens of mseca. Thus, in the vicinity of coastlines air-pressure-induced tilt may be expected to be extremely high.

Deformations due to seasonal air pressure variations

While the last section dealt with the atmospherical loading at periods in the range of several days, in this section the effects of seasonal air pressure variations will be estimated. It is well known that monthly mean values of air pressure can be roughly characterized by a standing wave with extreme values in winter and summer and zero points in spring and autumn. Hence, one can get an idea of the maximum air-pressure-induced deformation and gravity effects by comparing the states of deformation between January and July.

The corresponding difference in the air pressure distribution is shown in Fig. 6. It is tabulated in Munk and Macdonald (1960), with gridpoints spaced every 10° in latitude and 20° in longitude.

The Munk and Macdonald pressure maps have been convolved with the Green's functions for the Gutenberg-Bullen A Earth model to yield the differences in the state of deformation and gravity between January and July. Again, the inverse barometer response has been assumed for oceanic areas. The results of the convolution are presented in Figs. 7–11, showing maximum seasonal variations of more than 1 cm for vertical displacements, 1 mm for horizontal displacements, 3×10^{-9} for horizontal strain, nearly 6 μgal for gravity and around 3 mseca for tilt. In the case of horizontal displacements and tilt these extreme values are obtained for a region in the neighbourhood of Siberia and in the case of gravity the maximum value is

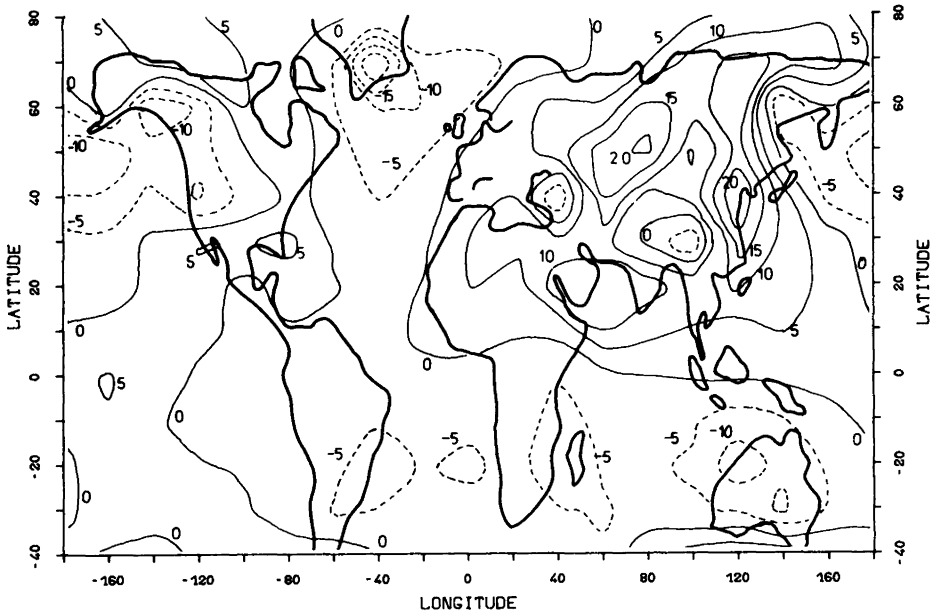

Fig. 6. Seasonal deviation of air pressure from atmospheric mean (mbar): "January minus July", according to Munk and Macdonald (1960)

obtained for Greenland. In all other cases they are valid for Siberia.

Air pressure corrections for radial displacement and gravity

Regarding the enormous precision and high stability of the superconducting gravimeter and the recent developments in precise point positioning with space methods, gravity changes and radial displacements seem to be the components of deformation in global geodynamics which require air pressure corrections most necessarily.

A simple procedure for correcting radial displacements is not yet available. Gravity records are usually corrected by using a regression coefficient around 0.3 μgal/mbar. However, it was pointed out in the previous section that there is no one such regression coefficient, but that the coefficient is critically dependent on the wavelength of the loading. This is demonstrated in Fig. 12 which shows the seasonal gravity changes of Fig. 10 as a function of the local air pressure changes. Deviations from the best fitting regression line exceed the 1 μgal level. If one considers that the internal precision of the superconducting gravimeter lies around a tenth of a microgal, the shortcoming of the above correction will immediately become obvious.

The same applies to the possible correction of the radial displacements by means of one regression coefficient. It is seen from Fig. 13 that the deviations from the best fitting regression line may be as high as 4 mm. At present this correction error may not be serious for many purposes. But it will be too high if NASA can realize its plan to detect vertical surface motions with millimetre-scale accuracies (Walter 1984).

In order to improve these air pressure corrections we have prepared Tables 1–3. They give the air pressure regression coefficients for radial displacements and for primary and secondary gravity changes, respectively, as a function of the characteristic radius r_0 of the pressure anomaly and as a function of position with respect to the centre of the anomaly. The pressure distributions are assumed to obey Eq. (1). The positions with respect to the centre are determined by the relative pressure amplitudes p/p_{max}.

Figures 14–16 show these regression coefficients graphically. For the radial displacements the coefficient changes from approximately -0.1 mm/mbar at $r_0 = 160$ km to -0.9 mm/mbar at $r_0 = 5{,}500$ km. For the primary gravity changes the coefficient lies between about 0.41 μgal/mbar and 0.31 μgal/mbar and for the secondary gravity changes the possible regression coefficients are between -0.02 μgal/mbar and -0.18 μgal/mbar. It is obvious from these numbers that, for an accurate air pressure correction, an estimate of the characteristic wavelength of the pressure perturbation is absolutely necessary. With such an estimate the use of Tables 1–3 will give better results than the simple correction with only one regression coefficient.

It should be mentioned, however, that in general the line of regression between air pressure and a deformation component does not go through the origin but has the form

$$w = C_1 p + C_2 p_{max} \tag{3}$$

(see also Figs. 12 and 13), where w stands for any of the components u, g_p or g_s and where C_1 and C_2 are coefficients slightly dependent on r_0 and p/p_{max}. Only the coefficient C_1 is given in Tables 1–3 and shown in Figs. 14–16. The constant term $C_2 p_{max}$ will disappear, if not the deformation component itself, but its difference between two points at the Earth's surface is considered. These points may even belong to different cyclones because the effective constant term is always the sum of the constant terms of all cyclones on the Earth's surface. Therefore, it is the same for every point on the surface. From Figs. 12 and 13 it is seen that in practice the shifts of the regression lines are very small. Thus, the consideration of differences between the displacements or gravity variations at two different points is only necessary if the required precision of the air pressure correction is in the millimeter range and a fraction of a microgal.

The use of Tables 1–3 for the correction of air pressure effects on radial displacements and gravity requires an estimate of the characteristic wavelengths contained in a pressure distribution. Besides involving a certain amount of subjectivity, such an estimation may also involve somewhat tedious processes like two-dimensional filtering, smoothing

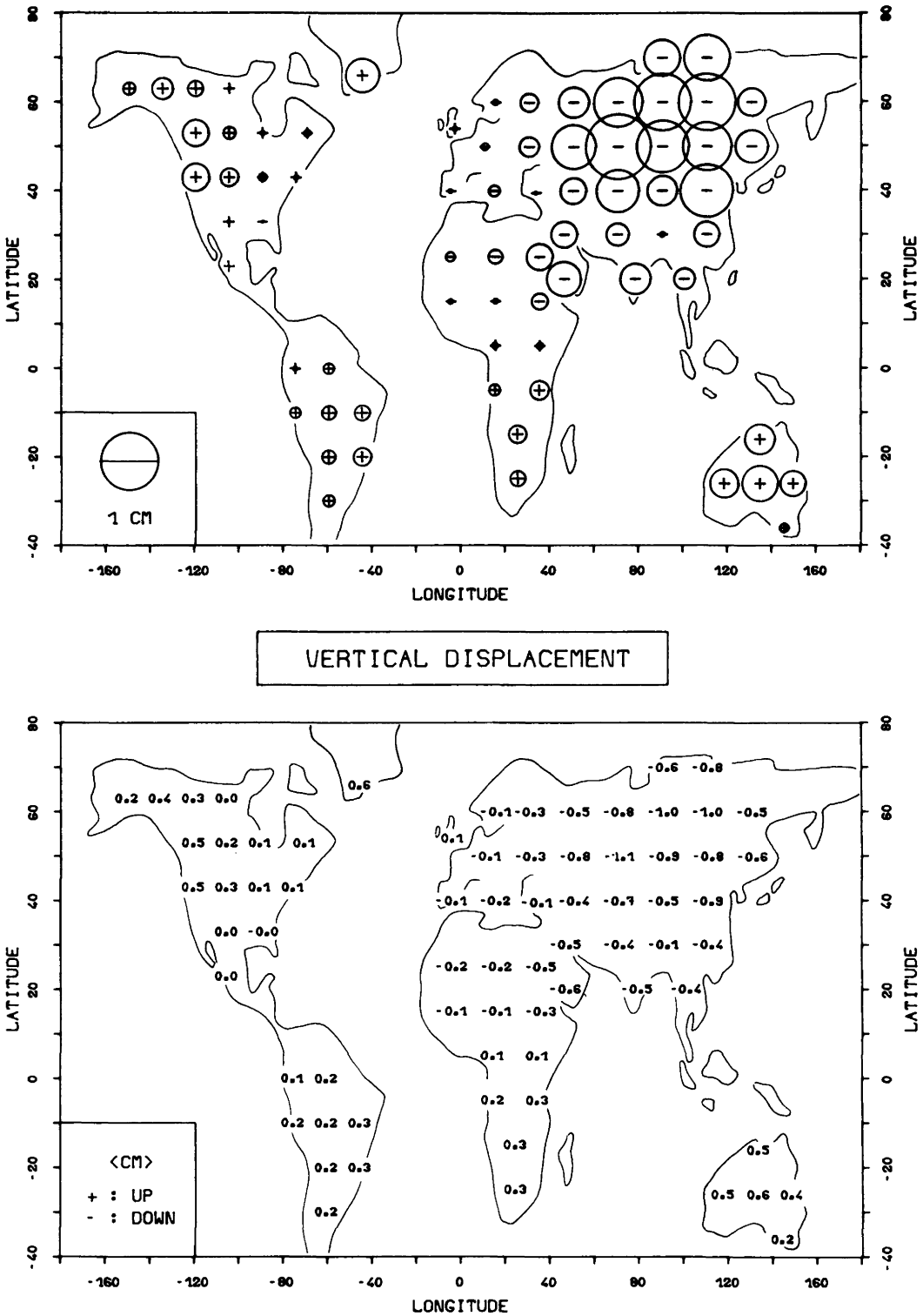

Fig. 7. Vertical displacements due to seasonal changes in the global air pressure distribution (Fig. 6): mean deviation "January minus July"

of the pressure distribution etc., which are not always easily done without a computer. We are therefore proposing a second and by far simpler method, which uses only two regression coefficients; one belonging to the long-wavelength loading and the other belonging to the short-wavelength loading. The proposed air pressure corrections are as follows:

$$\begin{aligned} &\text{Radial displacement:} && u = -0.90\,\tilde{p} - 0.35\,(p-\tilde{p}) \\ &\text{Primary gravity:} && g_p = 0.36\,\tilde{p} + 0.41\,(p-\tilde{p}) \\ &\text{Secondary gravity:} && g_s = -0.17\tilde{p} - 0.08\,(p-\tilde{p}) \\ &\text{Total gravity:} && g = g_p + g_s. \end{aligned} \qquad (4)$$

u will be in mm and the gravity values will be in μgal if the pressure values p, $\tilde{p}$, $\bar{p}$ are taken in mbar. p is the

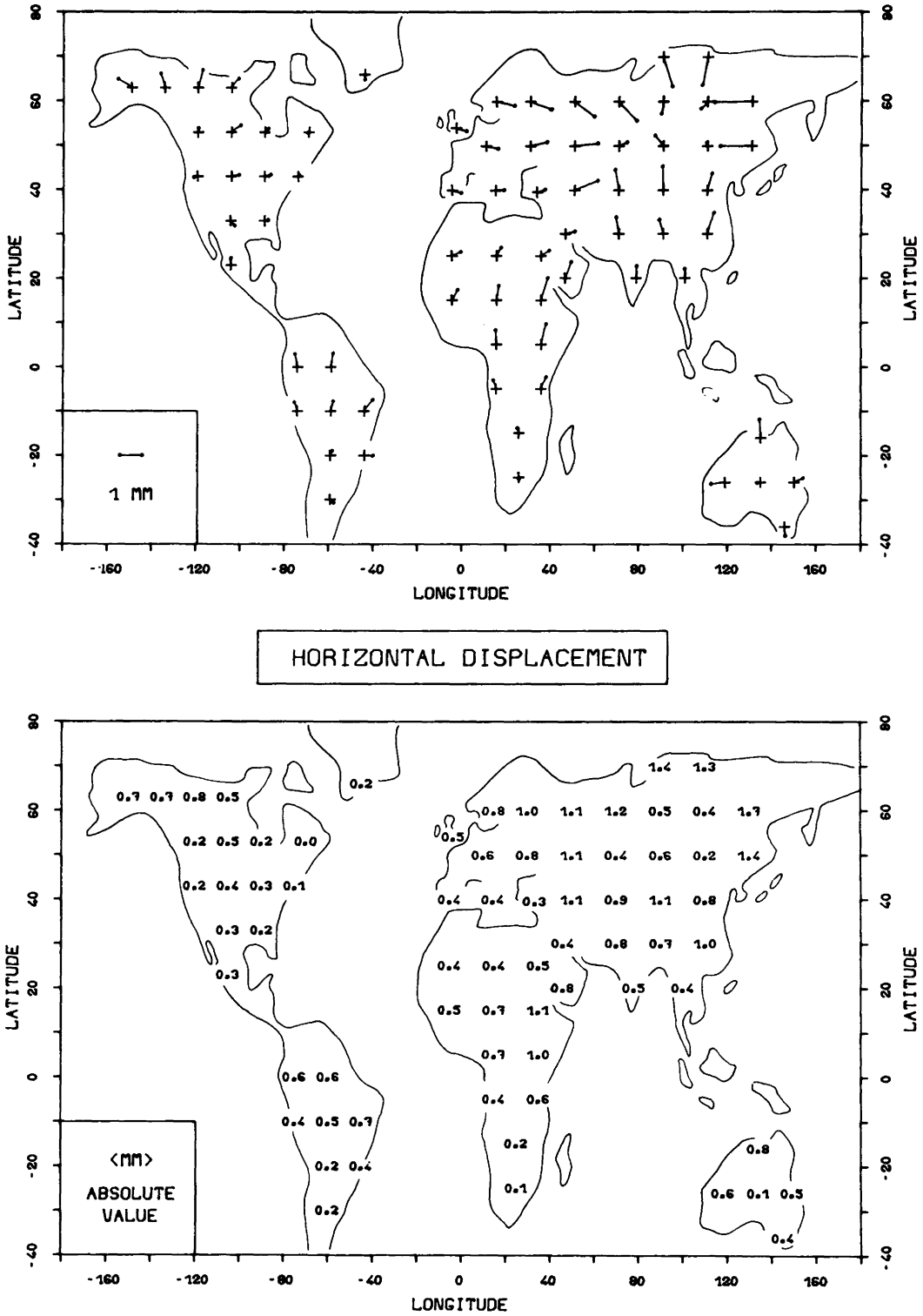

Fig. 8. Horizontal displacements due to seasonal changes in the global air pressure distribution (Fig. 6): mean deviation "January minus July"

measured pressure variation at the surface point under investigation. $\bar{p}$ denotes the long-wavelength component of the pressure variation. It is obtained by averaging the pressure variations in a surrounding area of 2,000 km. $\tilde{p}$ is obtained in the same way, except that the pressure changes for the ocean areas are set to zero. This is necessary in order to account for the inverse barometer effect of the oceans which influence the radial displacements and the secondary gravity changes.

We have applied the above empirical corrections to the seasonal variations of Figs. 6, 7 and 10. For averaging the pressure values we have used a $1{,}000 \times 1{,}000$ km^2 grid system consisting of 16 squares in each of which the average was estimated by inspection. The corrections determined

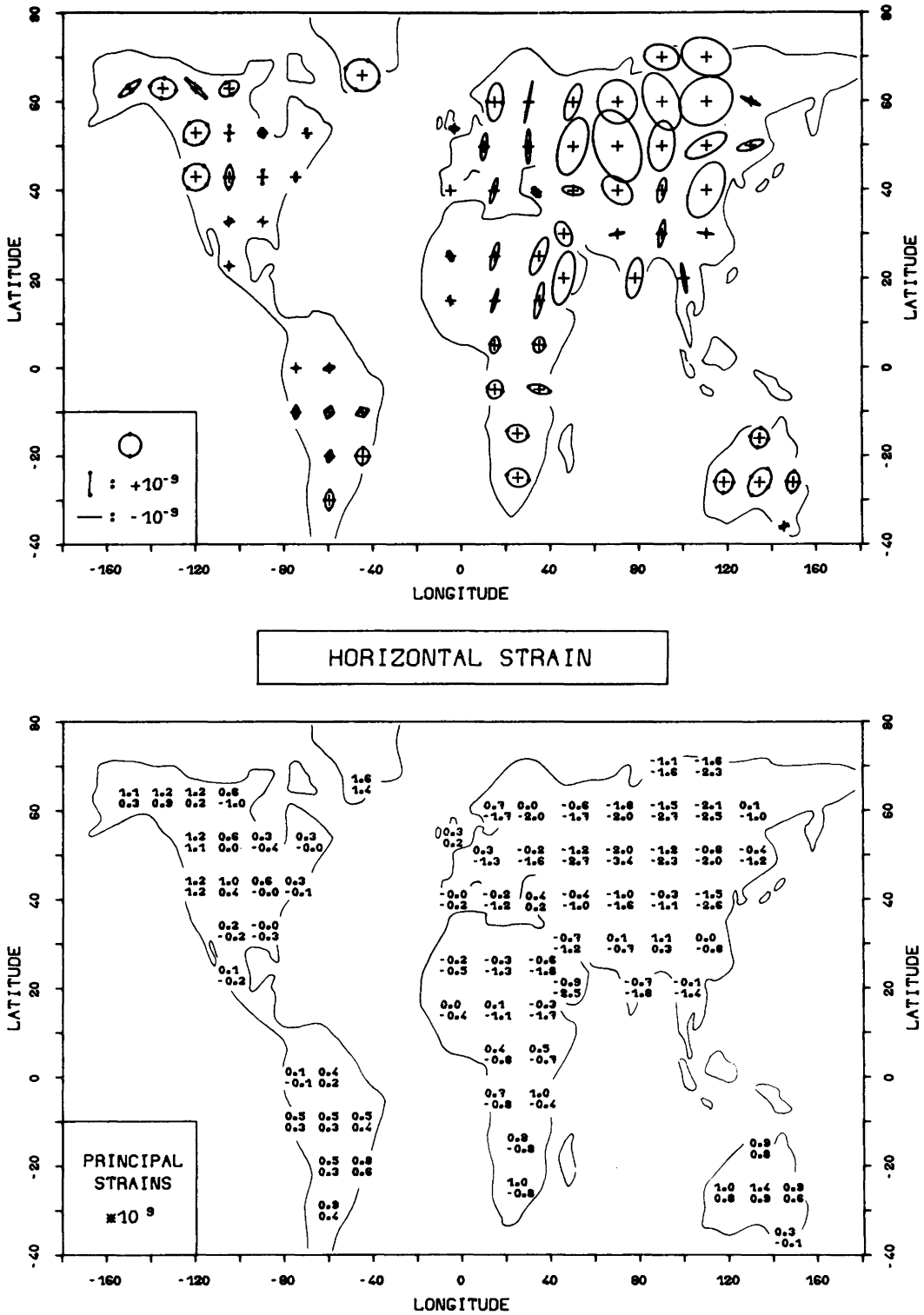

Fig. 9. Horizontal principal strains due to seasonal changes in the global air pressure distribution (Fig. 6): mean deviation "January minus July". *Top:* The principal horizontal strain components coincide with the principal axes of the ellipses. The length of the principal axes is proportional to the principal strains. *Dots* at the end of a principal axis denote dilatation, otherwise compression is meant. *Bottom:* " + " dilatation, " − " compression

in this way are compared in Figs. 17–20 with the corrections as obtained from exact loading calculations by means of Green's functions. Except for a small constant term there is excellent agreement between both. The mean differences are less than 0.5 mm, 0.1 μgal, 0.1 μgal and 0.2 μgal for the radial displacements, the primary, secondary and total gravity changes, respectively. At maximum, the error in the estimation of the air-pressure-induced radial displacements is ±1 mm. For the primary and secondary gravity changes the maximum estimation error is ±0.3 μgal and

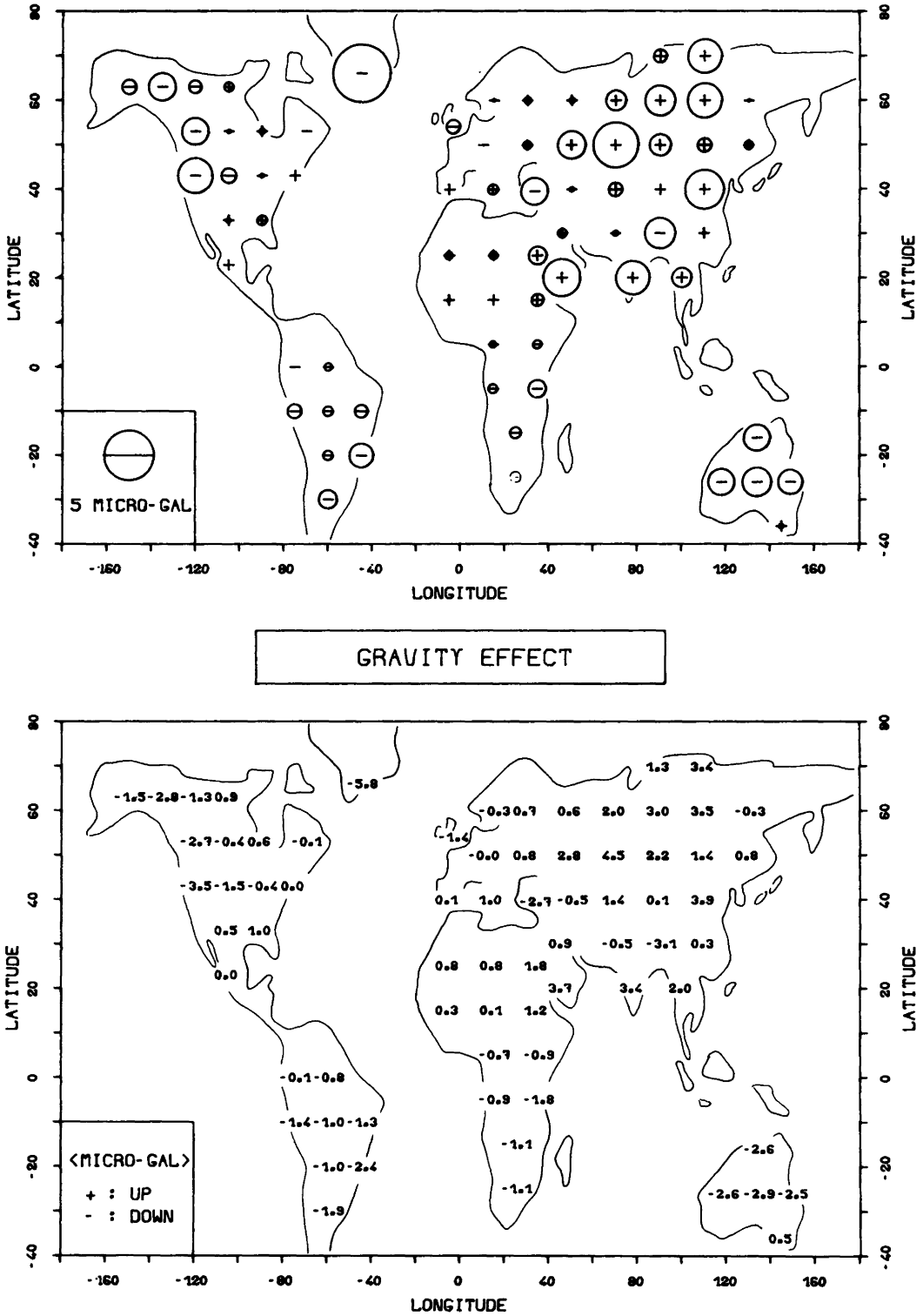

Fig. 10. Total gravitry effect due to seasonal changes in the global air pressure distribution (Fig. 6): mean deviation "January minus July". Gravity is positive upwards!

± 0.2 μgal, respectively, and for the total gravity changes ± 0.4 μgal. This does not take the constant term into account, which is due to distant pressure variations and which is the same for every point on the surface (see above). For the radial displacements it turns out to be practically zero (less than 0.1 mm), for the primary and secondary gravity changes its absolute value is less than 0.2 μgal and 0.1 μgal, respectively, and for the total gravity changes less than 0.3 μgal. As explained above, the constant term will not be important if gravity or displacement differences between two points on the Earth's surface are considered. The estimation errors involved in Eq. (4) are, on average, four times smaller than those obtained when using the best fitting line of regression between gravity changes and displacements

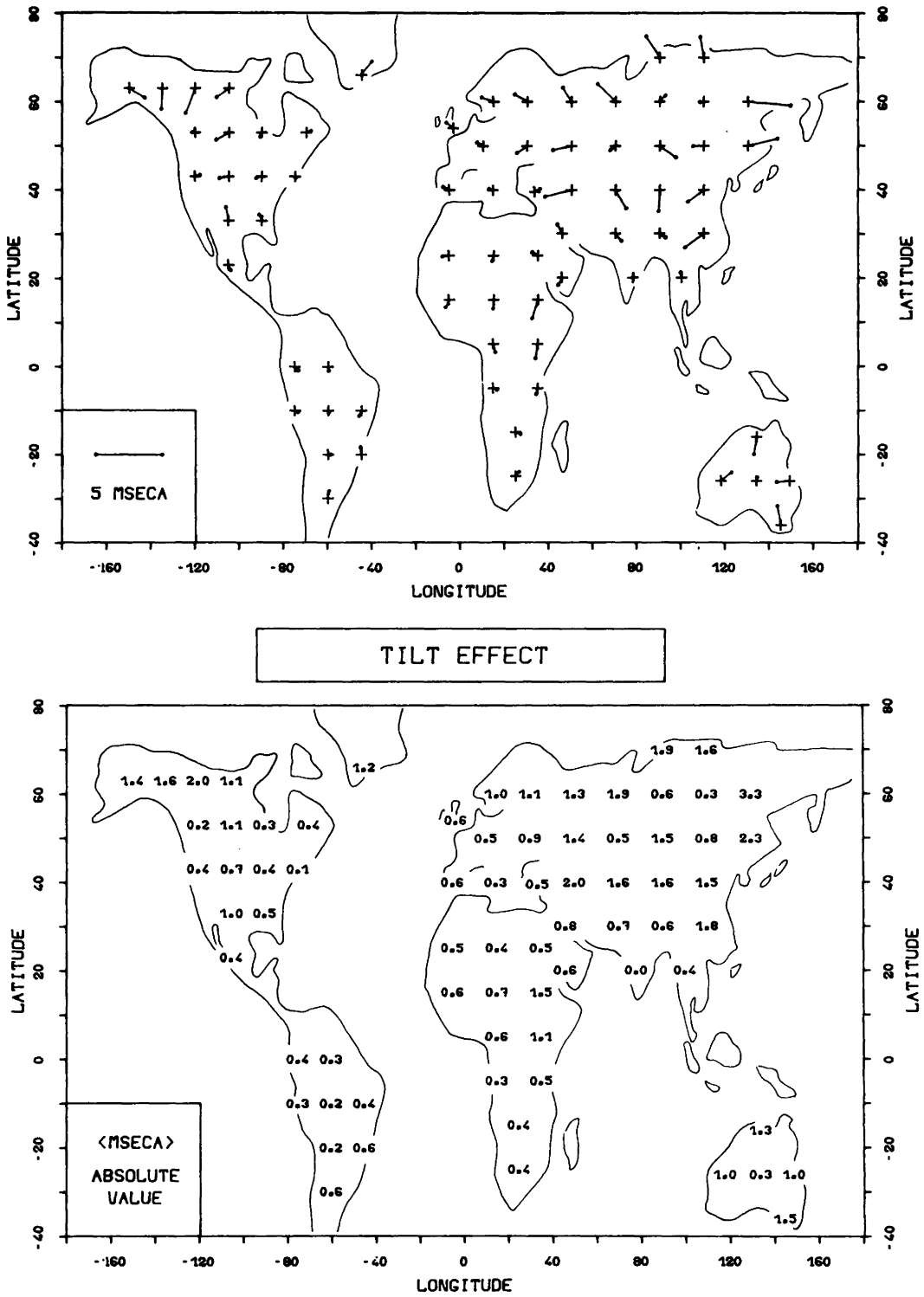

Fig. 11. Total tilt due to seasonal changes in the global air pressure distribution (Fig. 6): mean deviation "January minus July"

on the one hand and pressure variations on the other hand. Thus, the proposed correction method is not only simple but it is also highly precise and fulfils the present requirements of geodynamics.

Conclusions

The magnitude of air-pressure-induced deformation and gravity effects far from any coastline can reach more than 10% of the corresponding body tide effects. For tilt and strain the air pressure influence may even be of the same order of magnitude as the body tide. Maximum values are tabulated in Table 4.

These results have to be revised if the loading distribution is not continuous but contains a discontinuity due to the existence of a coastline. Vertical displacements, azimuthal strains and secondary gravity changes are slightly weakened near the coast, whereas all the other deformation

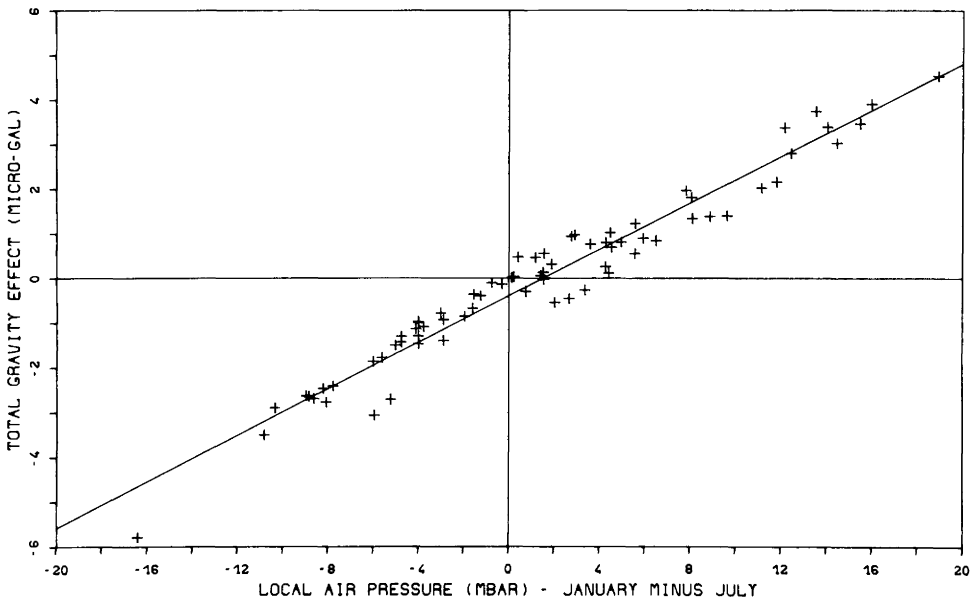

Fig. 12. Total gravity effect due to seasonal changes in the global air pressure distribution (Fig. 6) as a function of local air pressure. Deviations from the best fitting regression line exceed the 1 μgal level!

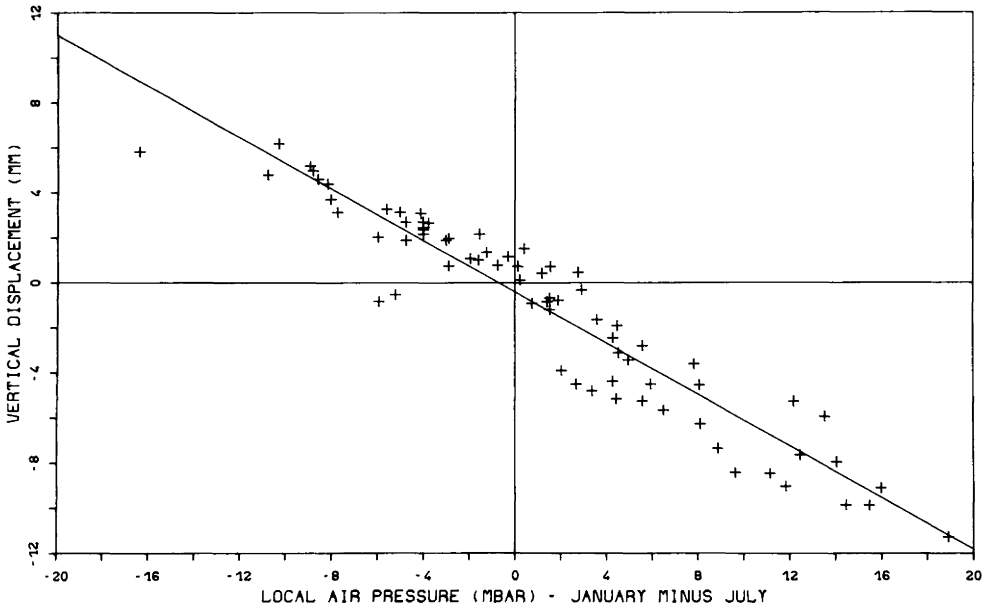

Fig. 13. Vertical displacement due to seasonal changes in the global air pressure distribution (Fig. 6) as a function of local air pressure. Deviations from the best fitting regression line may be as high as 4 mm!

components are amplified up to several hundred percent in the vicinity of coastlines, the amplification depending on the deformation components, geometry of the coastline, distance to the coastline and of course on the size and amplitude of the pressure anomaly itself. In addition, even the sign of a deformation component may change due to the existence of a coastline.

Further complications may arise from the dynamic reaction of the ocean to air pressure loading which was not taken into account here.

The vertical displacements in Table 4 coincide well with those given by Trubytsin and Makalkin (1976) who carried out analytical calculations for cyclones above a homogeneous half-space. They are also in good agreement with the seasonal vertical movements given by Stolz and Larden (1979). In all cases the displacements are of centimetre-order. This corresponds to the precision which is presently approached for the measurements of regional and global base lengths using geodetic space techniques such as VLBI (Very Long Baseline Interferometry) and Laser Ranging. Even millimetre-scale accuracies are already envisaged (Walter 1984). A correction of such measurements for air-

Table 1. Regression coefficient $C_1 = du/dp$ (mm/mbar) for vertical displacement [see Eq. (3)]. p: local pressure, P_{max}: maximum pressure at the centre of a cyclone, r_0: radius of a cyclone [see Eq. (1)]

P/P_{max} (%)	20	35	50	65	80	95
r_0 (km):						
160	−0.134	−0.114	−0.105	−0.099	−0.096	−0.092
300	−0.207	−0.182	−0.171	−0.156	−0.156	−0.148
450	−0.269	−0.236	−0.220	−0.214	−0.204	−0.198
600	−0.312	−0.280	−0.262	−0.251	−0.245	−0.238
800	−0.363	−0.329	−0.310	−0.296	−0.287	−0.283
1,000	−0.416	−0.371	−0.348	−0.335	−0.326	−0.319
1,300	−0.479	−0.425	−0.404	−0.385	−0.374	−0.368
1,600	−0.544	−0.481	−0.452	−0.435	−0.421	−0.412
2,000	−0.629	−0.557	−0.520	−0.495	−0.480	−0.469
2,500	−0.734	−0.646	−0.600	−0.572	−0.552	−0.537
3,000	−0.824	−0.726	−0.677	−0.644	−0.620	−0.606
3,500	−0.890	−0.794	−0.743	−0.710	−0.684	−0.668
4,000	−0.925	−0.846	−0.798	−0.766	−0.741	−0.724
4,500	−0.933	−0.878	−0.839	−0.809	−0.788	−0.773
5,000	−0.915	−0.890	−0.863	−0.842	−0.824	−0.813
5,500	−0.874	−0.885	−0.875	−0.862	−0.850	−0.843

Table 2. Regression coefficient $C_1 = dg_p/dp$ (μgal/mbar) for primary gravity [see Eq. (3)]. p: local pressure, p_{max}: maximum pressure at the centre of a cyclone, r_0: radius of a cyclone [see Eq. (1)]

p/p_{max} (%)	20	35	50	65	80	95
r_0 (km)						
160	0.4084	0.4041	0.4014	0.3996	0.3985	0.3932
225	0.4147	0.4081	0.4057	0.4059	0.4080	0.4090
450	0.4148	0.4107	0.4098	0.4155	0.4135	0.4096
600	0.4097	0.4114	0.4098	0.4106	0.4141	0.4113
800	0.4045	0.4091	0.4106	0.4095	0.4099	0.4125
1,000	0.4008	0.4052	0.4071	0.4082	0.4088	0.4093
1,300	0.3981	0.3989	0.4037	0.4034	0.4041	0.4068
1,600	0.3904	0.3936	0.3970	0.4001	0.4014	0.4019
2,000	0.3796	0.3876	0.3916	0.3929	0.3954	0.3969
2,500	0.3679	0.3776	0.3828	0.3861	0.3888	0.3891
3,000	0.3574	0.3679	0.3749	0.3784	0.3809	0.3833
3,500	0.3466	0.3585	0.3663	0.3712	0.3738	0.3765
4,000	0.3344	0.3497	0.3581	0.3635	0.3670	0.3693
4,500	0.3237	0.3407	0.3504	0.3557	0.3600	0.3632
5,000	0.3144	0.3320	0.3425	0.3489	0.3532	0.3569
5,500	0.3055	0.3239	0.3353	0.3421	0.3469	0.3502

Table 3. Regression coefficient $C_1 = dg_s/dp$ (μgal/mbar) for secondary gravity [see Eq. (3)]. p: local pressure, p_{max}: maximum pressure at the centre of a cyclone, r_0: radius of a cyclone [see Eq. (1)]

p/p_{max} (%)	20	35	50	65	80	95
r_0 (km)						
160	−0.0305	−0.0262	−0.0241	−0.0229	−0.0221	−0.0212
300	−0.0465	−0.0412	−0.0388	−0.0354	−0.0354	−0.0336
450	−0.0603	−0.0530	−0.0495	−0.0481	−0.0460	−0.0446
600	−0.0703	−0.0631	−0.0589	−0.0565	−0.0552	−0.0535
800	−0.0816	−0.0740	−0.0697	−0.0666	−0.0646	−0.0636
1,000	−0.0931	−0.0832	−0.0782	−0.0754	−0.0733	−0.0717
1,300	−0.1056	−0.0946	−0.0901	−0.0861	−0.0837	−0.0825
1,600	−0.1175	−0.1054	−0.0998	−0.0963	−0.0935	−0.0916
2,000	−0.1319	−0.1192	−0.1124	−0.1077	−0.1049	−0.1029
2,500	−0.1480	−0.1338	−0.1261	−0.1213	−0.1180	−0.1153
3,000	−0.1611	−0.1461	−0.1384	−0.1330	−0.1292	−0.1269
3,500	−0.1710	−0.1562	−0.1486	−0.1434	−0.1393	−0.1369
4,000	−0.1772	−0.1645	−0.1569	−0.1520	−0.1481	−0.1455
4,500	−0.1809	−0.1703	−0.1636	−0.1587	−0.1554	−0.1531
5,000	−0.1824	−0.1740	−0.1684	−0.1644	−0.1612	−0.1592
5,500	−0.1818	−0.1761	−0.1719	−0.1684	−0.1659	−0.1642

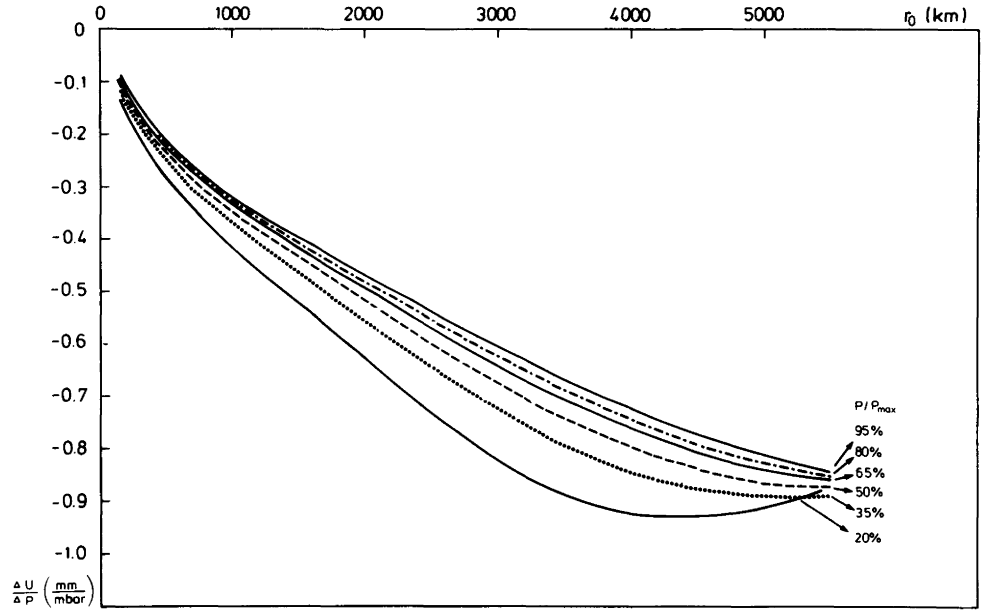

Fig. 14. Regression coefficient $C_1 = du/dp$ for vertical displacement [see Eq. (3)]. p: local pressure, p_{max}: maximum pressure at the center of a cyclone, r_0: radius of a cyclone [see Eq. (1)]

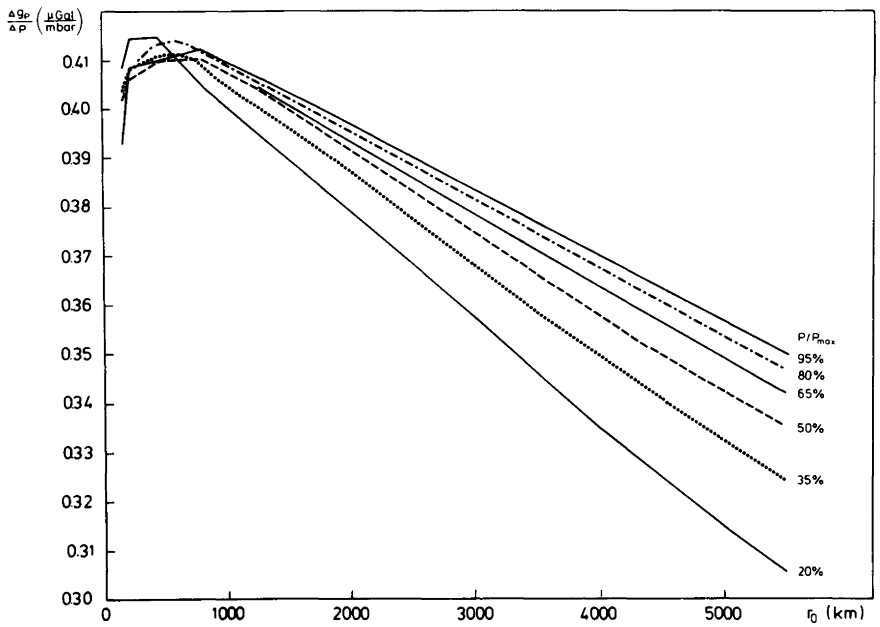

Fig. 15. Regression coefficient $C_1 = dg_p/dp$ for primary gravity [see Eq. (3)]. p: local pressure, p_{max}: maximum pressure at the centre of a cyclone, r_0: radius of a cyclone [see Eq. (1)]

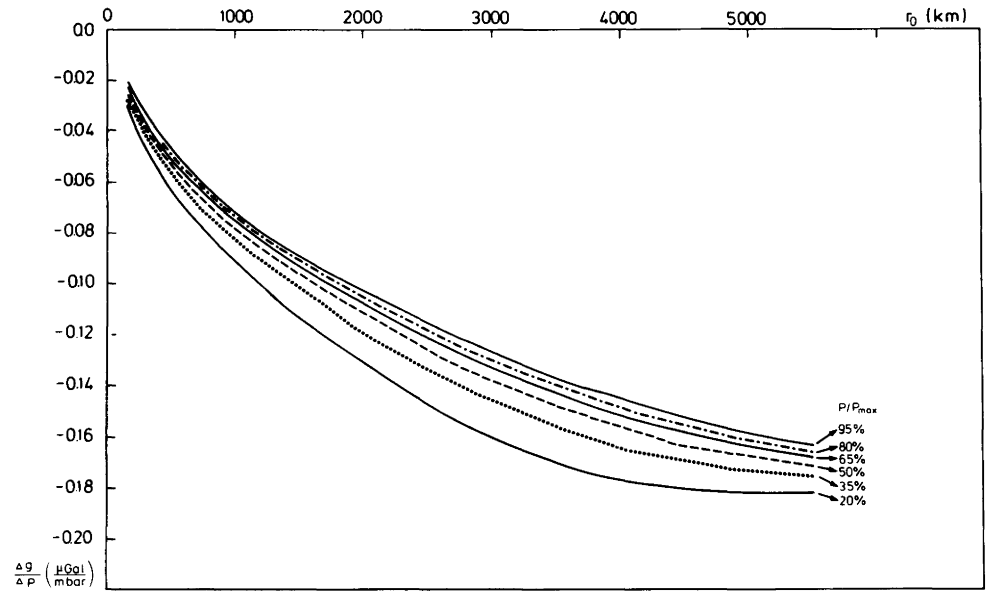

Fig. 16. Regression coefficient $C_1 = dg_s/dp$ for secondary gravity [see Eq. (3)]. p: local pressure, p_{max}: maximum pressure at the center of a cyclone, r_0: radius of a cyclone [see Eq. (1)]

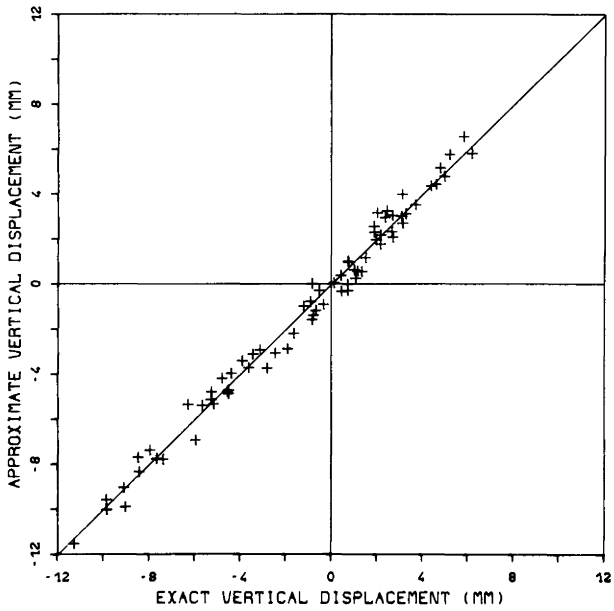

Fig. 17. Approximate vertical displacements according to Eq. (4) as a function of the corresponding values based on exact loading calculations. Results apply to seasonal changes in the global air pressure distribution shown in Fig. 6. Deviations from the exact calculations are less than 1 mm!

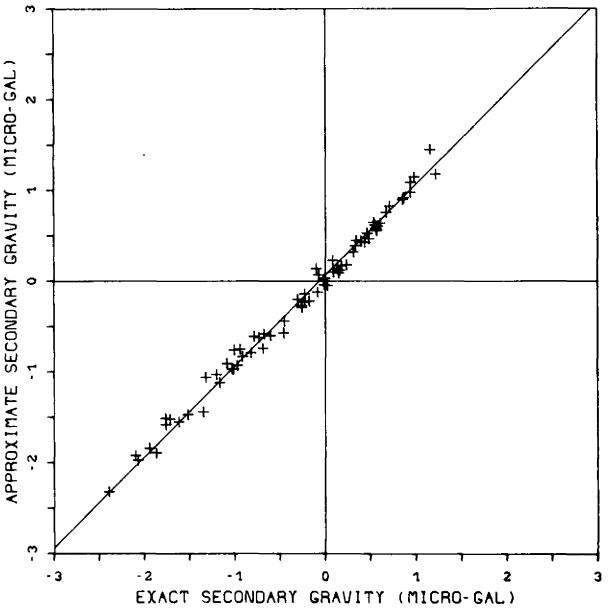

Fig. 19. Approximate secondary gravity effect according to Eq. (4) as a function of the corresponding values based on exact loading calculations. Results apply to seasonal changes in the global air pressure distribution shown in Fig. 6. Deviations from the exact calculations are less than 0.2 μgal!

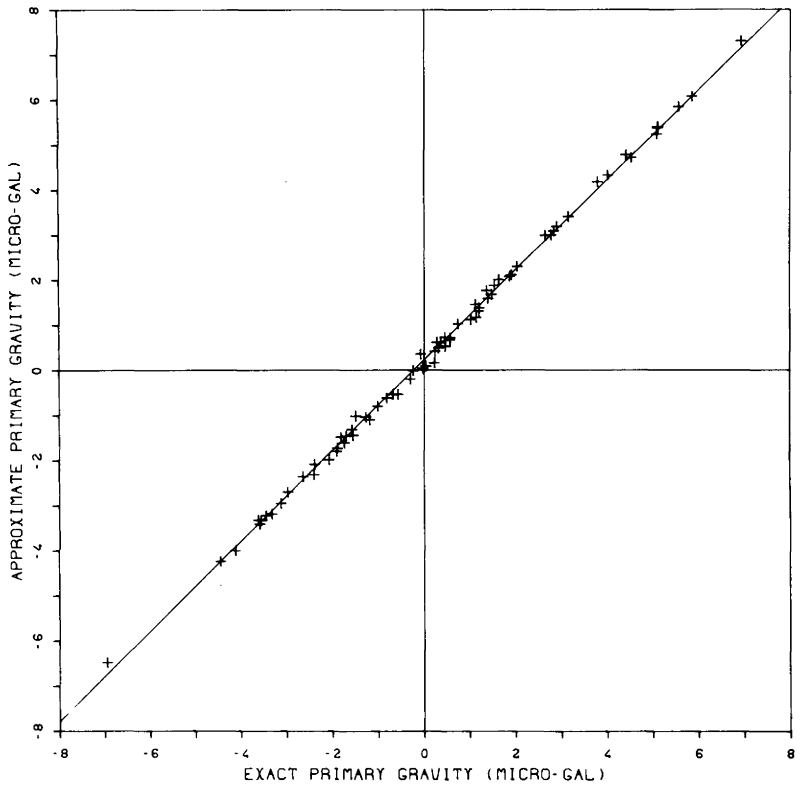

Fig. 18. Approximate primary gravity effect according to Eq. (4) as a function of the corresponding values based on exact loading calculations. Results apply to seasonal changes in the global air pressure distribution shown in Fig. 6. Deviations from the exact calculations are less than 0.3 μgal!

pressure-induced vertical displacements may therefore become desirable in the very near future. Air-pressure-induced horizontal displacements, however, seem to be negligible.

Although these results presented for vertical displacements seem to require an air pressure correction of regional and global base length measurements, such a correction does not appear to be easy. Scherneck (1983) proposes to use gravimeter recordings in order to correct global baseline measurements for loading tide vertical displacements. He comes up with a regression coefficient of approximately 0.4 cm/μgal for loading tides within a distance of 2,000 km. In the air pressure problem, such a regression coefficient

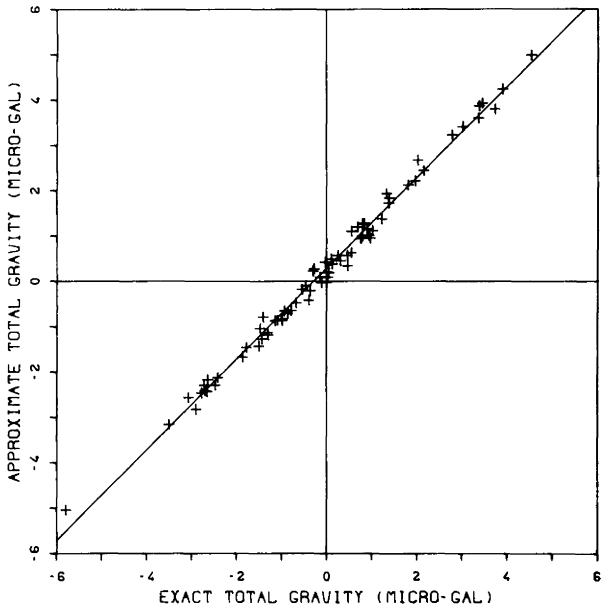

Fig. 20. Approximate total gravity effect according to Eq. (4) as a function of the corresponding values based on exact loading calculations. Results apply to seasonal changes in the global air pressure distribution shown in Fig. 6. Deviations from the exact calculations are less than 0.4 μgal!

Table 4. The Earth's response to deviations of air pressure from mean atmospheric pressure. (Values are approximate maximum values. They may have to be modified near coastlines)

Period	Some days	One year
Pressure variation (mbar)	± 60	± 10
Vertical displacement (cm)	∓ 2.5	∓ 0.5
Horizontal displacement (mm)	± 2.5	± 0.5
Horizontal strain ($*10^9$)	∓ 10	∓ 1.5
Gravity effect (μgal) (positive upwards)	± 20	± 3
Tilt effect (mseca)	± 10	± 1.5

can only be given reliably for the relation between air-pressure-induced displacements and the *secondary* gravity effect. The *primary* gravity effect which is the dominant one, does not correlate well enough with the displacements. A sufficient correction of base-length measurements using gravity recordings would therefore require the separation of the secondary gravity effect from the primary one. This, however, can probably not be done accurately enough at present.

The use of the wavelength dependent regression coefficients given in Tables 1–3 is more accurate. However, it involves the estimation of characteristic wavelengths and their amplitudes in a pressure distribution, which may be laborious in many cases. The use of Eq. (4) seems to be more adequate. It only involves two regression coefficients and needs a wheather-chart covering the surrounding area of 2,000 km around the surface point under investigation. The procedure of the air pressure correction is very simple and does not need any computer. Nevertheless, it is highly precise, allowing correction of seasonal radial displacements with an accuracy of at least 1 mm.

Among all continuous recording ground-based geodynamic instruments such as gravimeters, tiltmeters and strainmeters, probably the only one for which the long-term stability is good enough to reliably measure the small rates of tectonic movements is the superconducting gravimeter. Such movements may result in a few microgal gravity change within one year. Comparing this with the ± 20 μgal gravity perturbation within some days and ± 3 μgal within one year which may be introduced by air pressure variations, it is immediately clear that, besides air pressure corrections of radial displacements, such corrections are also necessary for gravity changes. Again the use of Eq. (4) seems to be most adequate for this purpose. It can provide air pressure corrections of seasonal gravity changes within ± 0.4 μgal.

Acknowledgements. We are grateful to L. Bittner, P. Sadowiak and A. Wahlen for the preparation of the figures and to K. Helbig for typing the manuscript.

References

Alterman, Z., Jarosch, H., Pekeris, C.L.: Propagation of Rayleigh waves in the Earth. Geophys. J.R. Astron. Soc. **4**, 219–241, 1961

Baur, F.: Einführung in die Großwetterkunde. Wiesbaden: Dieterichsche Verlagsbuchhandlung 1948

Committee on Geodesy, National Research Council: Geodetic monitoring of tectonic deformation – toward a strategy. Washington D.C.: National Academy Press 1981

Dziewonski, A.M., Anderson, D.L.: Prelimary reference Earth model. Phys. Earth Planet. Inter. **25**, 297–356, 1981

Farrell, W.E.: Deformation of the Earth by surface loads. Rev. Geophys. Space Phys. **10**, 761–797, 1972

Faust H.: Der Aufbau der Erdatmosphäre. Braunschweig: Vieweg, 1968

Longman, J.M.: A Green's function for determining the deformation of the Earth under surface mass loads. J. Geophys. Res. **67**, 845–850, 1962

Müller, T., Zürn, W.: Observation of gravity changes during the passage of cold fronts. J. Geophys. **53**, 155–162, 1983

Munk, W.H., Macdonald, G.J.F.: The rotation of the Earth. Cambridge University Press, 1960

Okubo, S.: Theoretical and observed Q of the Chandler Wobble – Love number approach. Geophys. J.R. Astron. Soc. **71**, 647, 1982

Prothero, W.A., Goodkind, J.M.: Earth-tide measurements with the superconducting gravimeter. J. Geophys. Res. **77**, 926–936, 1972

Scherneck, H.G.: Crustal loading affecting VLBI sites. Department of Geodesy Report No. 20, University of Uppsala, 1983

Smith, M.O., Dahlen, F.A.: The period and Q of the Chandler Wobble. Geophys. J. Astron. Soc. **64**, 223–281, 1981

Spratt, R.J.: Modelling of the effect of atmospheric pressure variations on gravity. Geophys. J.R. Astron. Soc. **71**, 173–186, 1982

Stolz, A., Larden, D.R.: Seasonal displacement and deformation of the Earth by the atmosphere. J. Geophys. Res. **84**, 6185–6194, 1979

Thompson, K.R.: Regression models for monthly mean sea level. Marine Geodesy **2**, 269–290, 1979

Trubytsin, A.P., Makalkin, A.V.S.: Deformation of the Earth's Crust due to atmospherical cyclones. Izv. Acad. Sci. USSR, Phys. Solid Earth **12**, 343–344, 1976

Walter, L.S.: Geodynamics. Proceedings of a workshop held at the Airlie House, Airly, Virginia, February 15–18, 1983; NASA Conference Publication 2325, 1984

Warburton, J.R., Goodkind, J.M.: The influence of barometric pressure variations on gravity. Geophys. J.R. Astron. Soc. **48**, 281–292, 1977

Zschau, J.: Auflastgezeiten. Habilitation-thesis. University of Kiel, 1979a

Zschau, J.: Phase shifts on tidal sea load deformations of the Earth's surface due to low viscosity layers in the interior. Proceed. 8th Intern. Symp. Earth Tides. 372–398, Bonn 1979c

Zschau, J.: Tidal friction in the solid Earth: Loading tides versus body tides. Proceed. 8th Intern. Symp. Earth Tides. 62–94, Bonn 1979d

Zschau, J.: The influence of the Earth's viscosity on deformations by marine tidal surface loads. In: Earth Rheology, isostasy and eustasy. N.-A. Mörner (ed): pp 161–167. John Wiley and Sons, 1980

Received January 31, 1984; revised version November 27, 1984
Accepted November 30, 1984